Origin of reentrant relaxor formation in ferroelectric solid solutions

Zhengkai Hong,[1] Ben Tian,[1] Xiaoqin Ke [1,*] Sen Yang,[1] and Yunzhi Wang [2,†]

[1]*School of Physics, MOE Key Laboratory for Nonequilibrium Synthesis and Modulation of Condensed Matter,*
Xi'an Jiaotong University, Xi'an 710049, China
[2]*Department of Materials Science and Engineering, The Ohio State University, Columbus, Ohio 43210, USA*

Nanoscale compositional heterogeneity created by doping in ferroelectric systems leads to the formation of conventional relaxors in most cases, but reentrant relaxors in some unusual cases. It has remained a long-standing puzzle why reentrant relaxors rather than conventional relaxors form in these unusual cases. In this study, we use a binary ferroelectric system having a solid solution of a ferroelectric with cubic (C) to tetragonal (T) transition at one end and a ferroelectric with C to rhombohedral (R) transition at the other end, with nanoscale compositional heterogeneities, to reveal the origin of the reentrant relaxor transition. Our phase field simulations based on Landau theory demonstrate that the reentrant relaxor transitions in such a system are manifested by the formation of R nanodomains in the T microdomains upon cooling at compositions near the T/R phase boundary, which is accompanied by frequency-dependent permittivity peaks below T_C. We found that the difference in phase transition sequence at different local compositions near the T/R phase boundary created by point defect doping is essential for the formation of reentrant relaxors. This work unravels the general conditions for the formation of reentrant relaxors and may shed light on the origin of other reentrant ferroic glasses.

I. INTRODUCTION

Point defects can disrupt the long-range order in domain structures of ferroic (ferroelectric, ferromagnetic, and ferroelastic) materials and produce two distinct types of "glassy" state, i.e., conventional ferroic glass (CFG) (such as relaxor, spin glass, and strain glass) and reentrant ferroic glass (RFG) (such as reentrant relaxor, reentrant strain glass, and reentrant spin glass) [1,2]. Both CFG and RFG have attracted much attention during the past 50 years because they not only show intriguing complex physics [3,4] but also exhibit many fascinating properties that rarely exist in their long range ordered ferroic domain structural states, such as the ultrahigh piezoelectric d_{33} coefficient of relaxors [5], superelastic behavior over a wide temperature range in strain glasses [6], high energy density of reentrant relaxors [7], large exchange bias effect in reentrant spin glasses [8], etc. The difference between CFG and RFG is that upon cooling the former directly develops from the disordered parent phase (paraelectric, paramagnetic, or austenite) while the latter develops from a high-temperature ferroic phase (ferroelectric, ferromagnetic, or martensitic) with long range ordered domain structures, i.e., reenters from a long range ordered ferroic state into a glassy ferroic state. To form CFG as well as RFG, it is essential to dope a sufficient amount of impurities into normal ferroelectrics; these impurities inevitably lead to nanoscale compositional heterogeneities because of their random spatial distribution. Normally, the nanoscale compositional heterogeneities could result in variation in local

ferroic phase transition temperatures [local transition temperature effect (LTTE)] and/or local strain/electric/magnetic fields [local field effect (LFE)], which disrupt the formation of long range ordered ferroic domains and lead to the formation of nanoscale ferroic domains, i.e., a ferroic glassy state, in CFG [9–13]. However, at some unusual cases, RFG rather than CFG forms in doped ferroic systems and the above-mentioned LTTE and LFE induced by the nanoscale compositional heterogeneity seem insufficient to explain why a short range ordered glassy state forms from a long range ordered ferroelectric state upon cooling in RFG. Thus, there must be something else that plays an important role in the formation of RFG as compared to CFG. Despite intensive research on RFGs over the past 50 years [14–20], however, it is still unclear what other conditions have to be met in order to form RFG.

In this study we hypothesize that reentrant relaxors appear at *interferroelectric phase boundaries* with *local compositional heterogeneities*. The local compositional heterogeneity then not only could produce the LTTE and LFE mentioned above, but could also generate a unique local effect, i.e., the *local transition sequence effect* (LTSE). Therefore, at interferroelectric phase boundaries, upon cooling, some local compositions would further undergo interferroelectric phase transition after the paraelectric-ferroelectric transition occurring for all local compositions, leading to the formation of reentrant relaxors. To test this hypothesis, we consider a perovskite-structured binary ferroelectric system containing an interferroelectric tetragonal (T)/rhombohedral (R) phase boundary; i.e., the two ends of the system have paraelectric cubic (C) to ferroelectric T and paraelectric C to ferroelectric R transitions, respectively, at their Curie temperatures, and at the intermediate compositions C to T to R transition

*kexiaoqin@mail.xjtu.edu.cn
†wang.363@osu.edu

occurs. We formulate a phase field model to account for the local compositional heterogeneity associated with randomly distributed substitutional ions, which can produce variations in local phase transition temperature and sequence (i.e., C to T, C to R, or C to T to R), as well as in the local electric field. By carrying out systematic phase field simulations, we establish a phase diagram containing normal ferroelectric, reentrant relaxor, and conventional relaxor. The simulations also reproduced all the unique characteristics of reentrant relaxors found in experiments, i.e., the formation of glassy nanodomains in long range ordered ferroelectric microdomains, and the frequency-dispersive dielectric-permittivity peaks followed by the frequency-independent peaks at Curie temperature upon cooling. We found that reentrant relaxors form at the interferroelectric T/R phase boundary because at this boundary the local composition variation would lead to T to R transition at only some local compositions upon further cooling after the C to T ferroelectric transition at all local compositions has completed at a higher temperature, leading to the formation of R nanodomains inside T microdomains. In other words, the LTSE associated with the interferroelectric T/R phase boundary and local composition heterogeneity, i.e., C to T transition at some local compositions but C to T to R transition at some other local compositions upon cooling, play indispensable roles in the formation of reentrant relaxors. Thus, this work unravels the origin of the formation of reentrant relaxors and may shed light on the origin of other RFGs such as reentrant spin glass as well. The ferroelectric state phase diagram established may guide the design of RFGs.

II. PHASE FIELD MODEL

The model perovskite-structured ferroelectric system considered in this study is a ferroelectric with a cubic (C, $Pm\bar{3}m$) to tetragonal (T, $P4mm$) transition substituted by a ferroelectric with cubic (C, $Pm\bar{3}m$) to rhombohedral (R, $R3m$) transition. At intermediate compositions of the system, C-T-R transition occurs. The doped substitutional ions having an average concentration of $\bar{c}$ are assumed randomly distributed in the system and, thus, the local ion concentration fluctuates around $\bar{c}$ with a Gaussian distribution, as illustrated in the Supplemental Material [21] (see also Refs. [22,23] therein). The local compositional heterogeneity would result in three local effects (LTTE, LTSE, and LFE), in which the former two are due to the compositional dependency of phase transition temperature and sequence while the latter one is caused by the charge imbalance of substitutional ions with host ions. The magnitude of the local electric field is assumed to be proportional to the local concentration c (i.e., $|E_{\text{local}}| = \lambda c$, where $\lambda = 65$ kV/cm [13,24]), and the direction is set to be random [24,25]. The concentration-dependent phase transition temperature and sequence are determined by the bulk chemical free energy given below.

The domain structure of the model ferroelectric system is described by the spatial-dependent distribution of spontaneous polarization $\mathbf{P} = [P_1, P_2, P_3]$. The total free energy of the system consists of the bulk chemical free energy, the gradient energy, the electrostatic energy, and the elastic energy [26,27],

$$F = \int_V (f_{\text{bulk}} + f_{\text{grad}} + f_{\text{elec}} + f_{\text{elas}})dV, \tag{1}$$

where V is the volume; f_{bulk}, f_{grad}, f_{elec}, and f_{elas} are the bulk free energy density, the gradient energy density, the electrostatic energy density and the elastic energy density, respectively, and they are all written as a function of polarization $\mathbf{P}$. The bulk free energy density, f_{bulk}, is approximated by a sixth-order Landau polynomial:

$$
\begin{aligned}
f_{\text{bulk}} = {} & A_1 \sum_{i=1}^{3} P_i^2 + A_{11} \sum_{i=1}^{3} P_i^4 + A_{111} \sum_{i=1}^{3} P_i^6 + A_{12} \\
& \times \sum_{i,j=1,2,3}^{i \neq j} P_i^2 P_j^2 + A_{112} \sum_{i,j=1,2,3}^{i \neq j} P_i^4 P_j^2 + A_{123} P_1^2 P_2^2 P_3^2,
\end{aligned}
\tag{2}
$$

where A_1, A_{11}, A_{111}, A_{12}, A_{112}, and A_{123} are the Landau coefficients. The gradient energy density, f_{grad}, can be written as

$$
\begin{aligned}
f_{\text{grad}} = {} & \frac{1}{2} G_{11} \sum_{i=1,2,3} P_{i,i}^2 + G_{12} \sum_{i<j} P_{i,j} P_{j,i} \\
& + \frac{1}{2} G_{44} \sum_{i<j} (P_{i,j} + P_{j,i})^2 + \frac{1}{2} G'_{44} \sum_{i<j} (P_{i,j} - P_{j,i})^2,
\end{aligned}
\tag{3}
$$

where G_{11}, G_{12}, G_{44}, and G'_{44} represent the gradient coefficients and $P_{i,j}$ denotes $\frac{\partial P_i}{\partial x_j}$. For simplicity, here the domain wall energy is set to be isotropic. Thus, the gradient energy density f_{grad} is calculated by

$$f_{\text{grad}} = \frac{1}{2} G_{11} \sum_{i=1,2,3;\, j=1,2,3} P_{i,j}^2. \tag{4}$$

The electric energy density f_{elec} is decomposed into the following four parts:

$$
\begin{aligned}
f_{\text{elec}} &= f_{\text{dipole}} + f_{\text{depol}} + f_{\text{local}} + f_{\text{appl}} \\
&= -\tfrac{1}{2} E_{i,\text{dipole}} P_i - \tfrac{1}{2} E_{i,\text{depol}} \overline{P}_i - E_{i,\text{local}} P_i - E_{i,\text{appl}} P_i,
\end{aligned}
\tag{5}
$$

where $E_{i,\text{dipole}}$ is the inhomogeneous electric field caused by dipole-dipole interactions, $E_{i,\text{depol}}$ is the average depolarization field, $E_{i,\text{local}}$ is the local electric field, and $E_{i,\text{appl}}$ is the external electric field. The details on the calculation of each part of the electric energy density are given in the Supplemental Material [21]. Note that the depolarization energy density f_{depol} is different under different electrical boundary conditions such as short-circuit boundary condition [28–31] and open-circuit boundary condition [32,33]; here the open-circuit boundary condition is employed. The elastic energy density f_{elas} is described by

$$f_{\text{elas}} = \tfrac{1}{2} C_{ijkl} e_{ij} e_{kl} = \tfrac{1}{2} C_{ijkl} (\varepsilon_{ij} - \varepsilon_{ij}^0)(\varepsilon_{kl} - \varepsilon_{kl}^0), \tag{6}$$

where C_{ijkl} is the elastic stiffness tensor, and e_{ij}, ε_{ij}, and ε_{ij}^0 denote the elastic strain, total strain, and spontaneous strain, respectively. ε_{ij}^0 is calculated by $\varepsilon_{ij}^0 = Q_{ijkl} P_k P_l$, where Q_{ijkl}
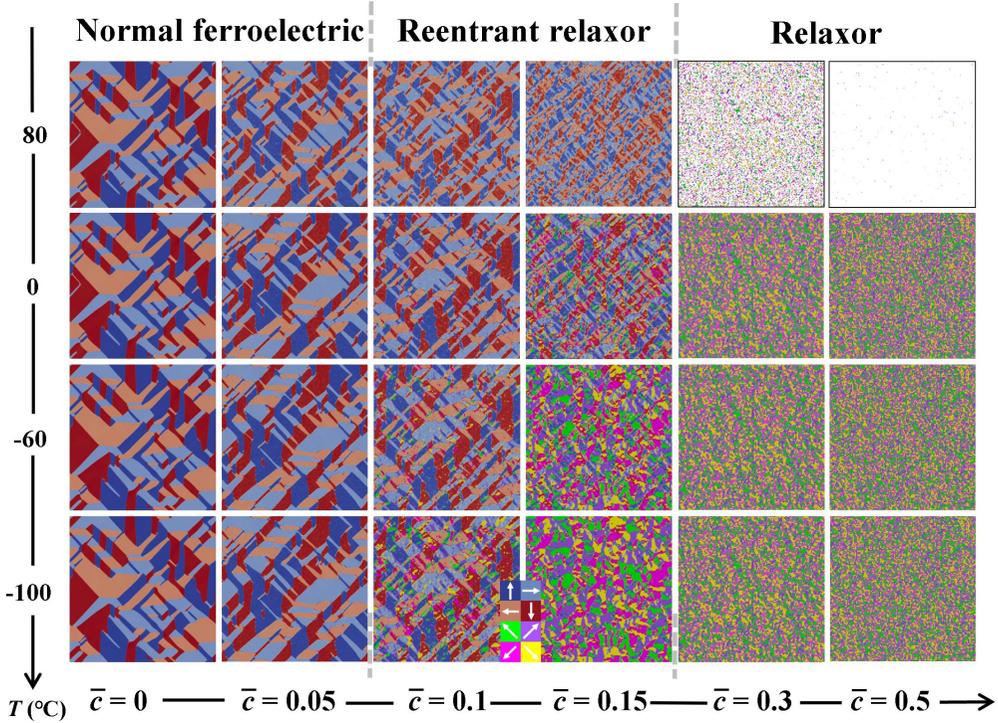
FIG. 1. Evolution of domain structure with temperature at different defect concentrations. The white region represents the paraelectric phase and the system is paraelectric phase at higher temperature ($T > 80°C$).

is the electrostrictive coefficient. The details on the calculation of elastic energy density are shown in the Supplemental Material [21].

The evolution of domain microstructure can then be obtained by solving the time-dependent Ginzburg-Landau equation,

$$\frac{\partial P_i(r, t)}{\partial t} = -M \frac{\delta F}{\delta P_i(r, t)} \quad (i = 1, 2, 3), \qquad (7)$$

where M is the kinetic coefficient and t is the time. The domain wall energy for 90° domain walls is assumed to be $0.01 \, \text{J/m}^2$ [34], which yields a length scale l_0 of ~ 1.2 nm. The simulation cell sizes are 512×512 [two-dimensional (2D)], which corresponds to a system with a size of $\sim 0.6 \times 0.6 \, \mu$m. The timescale $\Delta t = \frac{P^2 l_0}{M\gamma} = 5 \times 10^{-13}$ s in current simulations, where $M = 3 \times 10^4 \, \text{C}^2 \, \text{J}^{-1} \, \text{m} \, \text{s}^{-1}$ [34], $P = 0.45 \, \text{C m}^{-2}$ is the spontaneous polarization, l_0 is the length scale, and γ is the domain wall energy. The periodic boundary condition is applied along both dimensions. The parameters used in our phase field simulations are all given in the Supplemental Material [21]. The methods for calculating the heat capacity and the dielectric permittivity are introduced in Ref. [13].

III. RESULTS AND DISCUSSIONS

The evolution of ferroelectric domain structure with temperature decreasing at different $\bar{c}$ ($\bar{c} = 0.0, 0.05, 0.1, 0.15, 0.3$ and 0.5) is shown in Fig. 1. It is illustrated that the evolution of domain structure can be categorized into three types with the increase of $\bar{c}$: type I ($\bar{c} = 0.0, 0.05$, type II ($\bar{c} = 0.1, 0.15$, and type III ($\bar{c} = 0.3, 0.5$. For type I ($\bar{c} = 0.0$ and $\bar{c} = 0.05$, upon cooling, the system transforms from

the paraelectric C phase to ferroelectric T phase with microdomain structures, which indicates that the system undergoes a normal ferroelectric transition [35,36]. For type III ($\bar{c} = 0.3$ and $\bar{c} = 0.5$), upon cooling the system transforms from the paraelectric C phase to ferroelectric R phase with polar nanodomain structures, which suggests that the system undergoes a conventional relaxor transition [37]. For type II ($\bar{c} = 0.1$ and $\bar{c} = 0.15$), on the other hand, the system first transforms from the paraelectric C phase at high temperature to ferroelectric T phase with microdomain structures at low temperature, which is the characteristic of a normal ferroelectric transition. However, upon further cooling, R phase nanodomains nucleate and grow inside the T phase microdomains. Such a sequence of the polar domain structure evolution (type II), which is distinctively different from those of the normal ferroelectric transition and conventional relaxor transition, is a signature of the reentrant relaxor transition [38].

To further verify the formation of the reentrant relaxor at $\bar{c} = 0.1$ and 0.15, comparisons are made among the physical properties (temperature dependency of heat capacity and dielectric permittivity) of three representative compositions ($\bar{c} = 0.0$, $\bar{c} = 0.1$, and $\bar{c} = 0.3$) undergoing normal ferroelectric transition, reentrant relaxor transition, and conventional relaxor transition, respectively, which are illustrated in Fig. 2. As shown in Figs. 2(a1) and 2(a2), the normal ferroelectric transition occurring at T_C ($\sim 160°C$) of $\bar{c} = 0.0$ is further evidenced by the appearance of an obvious peak at T_C in the heat capacity–T curve [39], and the frequency-independent dielectric-permittivity peak at T_C [40]. As seen in Figs. 2(c1) and 2(c2), the conventional relaxor transition at $\bar{c} = 0.3$ is further confirmed by the absence of an obvious heat capacity
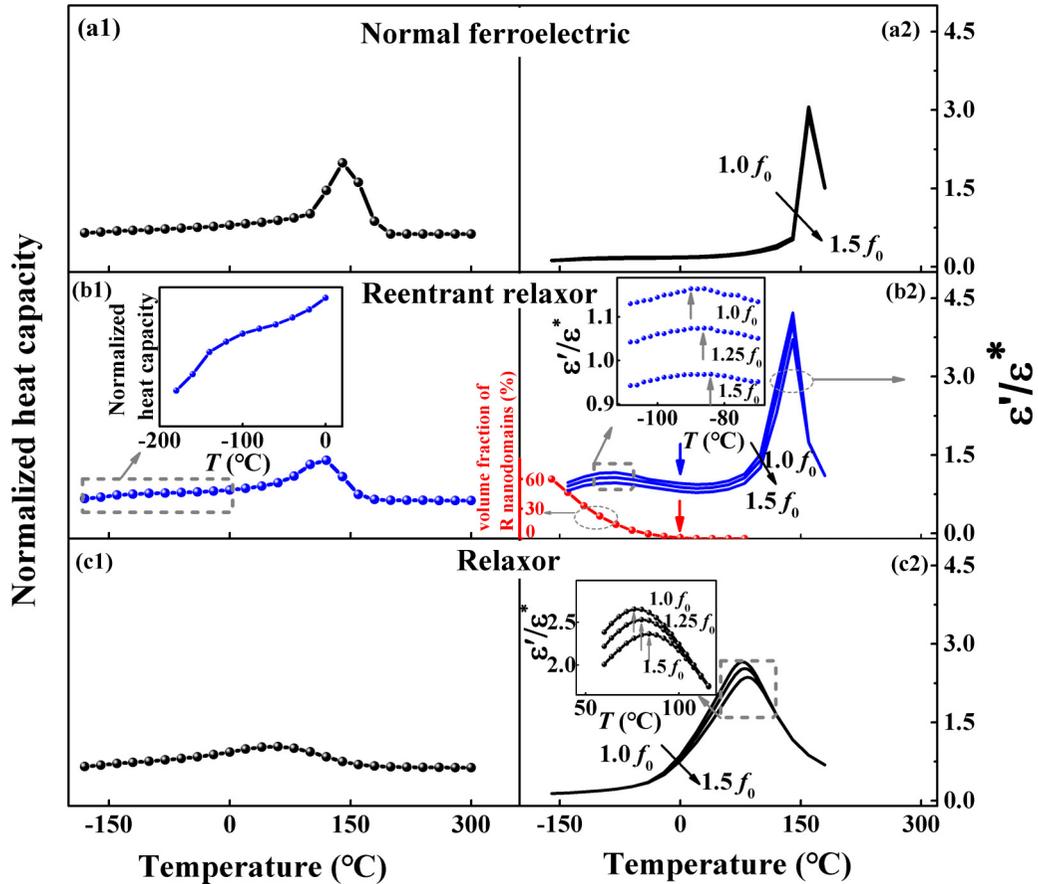
FIG. 2. Heat capacity–T curves (a1)–(c1) and dielectric permittivity–T spectrum (a2)–(c2) for $\bar{c} = 0.0$, $\bar{c} = 0.1$, and $\bar{c} = 0.3$. The variation of the volume fraction of R nanodomains with T for $\bar{c} = 0.1$ is shown by the red dotted line in (b2).

peak and the frequency-dependent dielectric-permittivity peaks [37]. On the other hand, the reentrant relaxor transition at $\bar{c} = 0.1$ is characterized by two unique features as shown in Figs. 2(b1) and 2(b2). Firstly, the heat capacity–T curve in Fig. 2(b1) exhibits a sharp peak at its T_C and then a diffused hump at lower temperatures [19]. Secondly, the dielectric permittivity–T curve in Fig. 2(b2) shows frequency-independent peaks at T_C and then frequency-dependent peaks (T_m) at lower temperatures, which agrees with the experimental results [7,38]. For the reentrant relaxor, at relatively high temperatures, the appearance of the heat capacity peak and the frequency-dependent peaks of dielectric permittivity are both indicative of a normal ferroelectric transition. On the other hand, at low temperatures, the diffused hump at the heat capacity–T curve along with the frequency-dependent permittivity peaks are associated with the appearance of R nanodomains (reentering into the glassy nanodomain state) for the reentrant relaxor. To prove this, Fig. 2(b2) gives the variation of the volume fraction of R nanodomains with temperature in the $\bar{c} = 0.1$ reentrant relaxor. It indicates that the temperature at which the dielectric permittivity–T curve of $\bar{c} = 0.1$ below T_C shows an inflection point (denoted by the blue arrow) coincides with the temperature at which the R nanodomains start to appear (denoted by the red arrow).

A phase diagram of the model system can then be constructed based on the dielectric permittivity–T curves of all

compositions considered [21], which is shown in Fig. 3(a). The phase diagram is composed of four regions, a paraelectric region, a ferroelectric region, a reentrant relaxor region, and a relaxor region. Figure 3(b) plots the phase diagram of the PbTiO$_3$−xBa(Ti$_{0.75}$Sn$_{0.25}$)O$_3$ system reported in the experiments [41]. It is seen that the topology of the calculated phase diagram resembles the experimentally measured one. In addition, other reentrant relaxor systems such as the BaTiO$_3$−5Bi−xSn system [38] and some typical reentrant spin glass systems such as Fe-xAu [3] and Co-xCu [42] exhibit similar phase diagram topology.

To unravel the mechanism underlying the formation of the reentrant relaxor, detailed analyses are made. Figure 4(a) shows the phase diagram plotted by considering a homogeneous system with only the bulk chemical free energy given in Eq. (1). It shows that within the studied temperature range, $c = 0.0 - 0.1$ compositions undergo C to T transition, $c = 0.1 - 0.2$ compositions undergo C-T-R transition and $c = 0.2 - 0.5$ compositions undergo C to R transition. From comparison with the phase diagram in Fig. 3(a), which takes into account the local compositional heterogeneity as well as the elastic, electrostatic, and gradient energy contributions in the system, it is readily seen that the reentrant relaxor transition mainly occurs at compositions with C-T-R transitions (i.e., the T/R phase boundary compositions). To understand why the reentrant relaxor occurs at the T/R phase
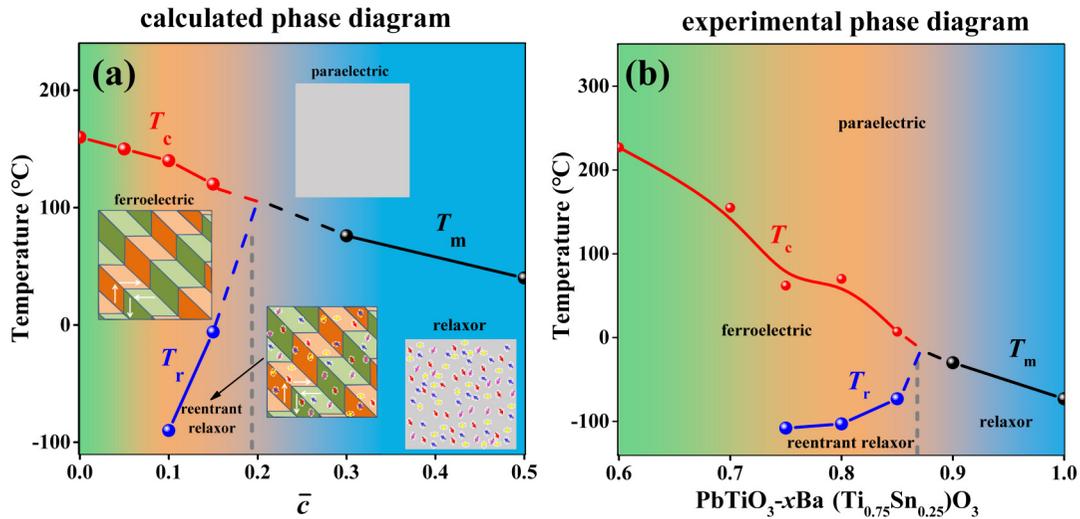
FIG. 3. (a) The calculated phase diagram of the model system. (b) Experimental reentrant relaxor phase diagram of $PbTiO_3 - xBa$ $(Ti_{0.75}Sn_{0.25})O_3$ [41].

boundary compositions, a reentrant relaxor system ($\bar{c} = 0.1$) and a conventional relaxor system ($\bar{c} = 0.3$) are compared. Figures 4(b1) and 4(b2) show the distribution of local compositions in the two systems, from which it is seen that local compositional heterogeneity exhibits in both systems. Figures 4(c1) and 4(c2) give the domain microstructures at $T = 20°C$ and $T = -100°C$ for $\bar{c} = 0.1$, respectively. It indicates that the system is occupied by T microdomains at $T = 20°C$ and R nanodomains start to occupy some locations of the T microdomains at $T = -100°C$. To find out why the R nanodomains appear at these locations and the T microdomains remain at other locations, the distributions of local compositions where the R nanodomains appear and local compositions where the T microdomains remain at $T = -100°C$ are plotted in Fig. 4(d2). It is demonstrated that on average, the R nanodomains appear at regions with higher doped ion content and the T microdomains remain at regions with lower doped ion content. Specifically, the remaining T phase domains are distributed at regions with lower average ion concentrations (~ 0.09) and the R phase domains are distributed at regions with higher average ion concentrations (~ 0.12). Figures 4(e4)–4(e6) compare the bulk chemical free energy of the T and R phases at different compositions at $T = -100°C$, which show that at low concentrations ($c < 0.1185$), the T phase has a lower free energy than that of the R phase while at higher concentrations ($c > 0.1185$), the R phase has a lower free energy. Therefore, it is clear that the R nanodomains nucleate and grow in the T microdomains because at some local compositions, the R phase is more stable than the T phase. Figures 4(e1)–4(e3) show the bulk chemical free energy curves of the T and R phases at different compositions at $T = 20°C$, which indicates that at this temperature, the T phase of all local compositions of the $\bar{c} = 0.1$ system has a lower bulk chemical free energy than the R phase does, which explains why at $T = 20°C$ no R nanodomains appear within the T microdomain. In contrast, for the relaxor system ($\bar{c} = 0.3$), although local compositional heterogeneity exists, the R phase is most stable for all local compositions as

shown in Figs. 4(d3) and 4(d4) and Figs. 4(e7)–4(e12). Thus, the reentrant relaxor could not occur.

Note that in this study, if the strength of the local field (i.e., λ) is increased, the T phase relaxor could be induced at high temperature for $\bar{c} = 0.1$ and then the T relaxor to R relaxor transition upon further cooling as reported in recent literature [43,44] rather than the T ferroelectric to R relaxor transition (i.e., reentrant relaxor) would occur.

Therefore, the nanoscale compositional heterogeneity around the T/R interferroelectric phase boundary in the phase diagram leads to the formation of the reentrant relaxor. The formation of R glassy nanodomains within the high-temperature T microdomains could be ascribed to the lower bulk chemical free energy of the R phase as compared to that of the T phase with decreasing temperature at some local compositions. The main driving force for the formation of the reentrant relaxor, thus, should be the reduction of the bulk chemical free energy.

The above mechanism of reentrant relaxor (i.e., nanoscale compositional heterogeneity combined with the inter-ferroelectric phase boundary) should be general and applicable to other reentrant relaxor systems such as $BaTiO_3 - 5Bi - xSn$ [38] and $Pb_{1-x}Ba_xNb_2O_6$ [45]. In the $Pb_{1-x}Ba_xNbO_6$ system, for example, the ferroelectric phase at the $PbNb_2O_6$ end is orthorhombic (O) ($Cm2m$) and the ferroelectric phase at the $BaNb_2O_6$ end is tetragonal ($P4bm$). The reentrant relaxor is reported to appear at $x = 0.385$ near the tetragonal-orthorhombic interferroelectric phase boundary, which could be a result of the local compositional heterogeneity combined with the variation of local phase transition sequences (C to T, and C to T to O) at different local compositions. In addition, the mechanism could also operate in other reentrant ferroic glasses such as reentrant spin glass (Fe-xAu [3] and Co-xCu [42]) that are frequently observed in doped ferromagnetic systems, although in reentrant spin glasses the two competing phases are normally ferromagnetic (FM) and antiferromagnetic (AFM) rather than two different ferroelectric phases.
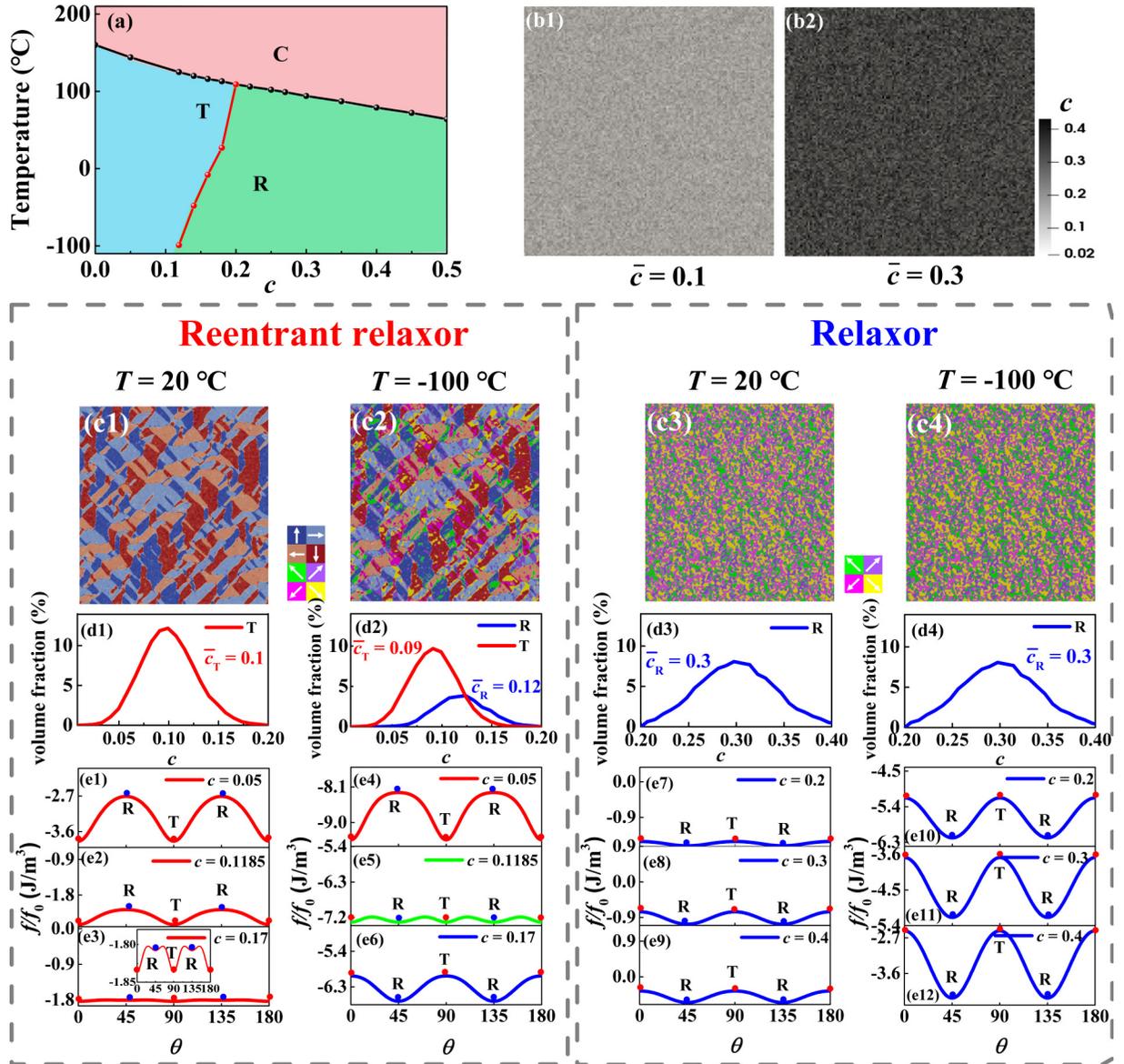
FIG. 4. (a) The calculated phase diagram of a homogeneous system considering only the bulk chemical free energy. (b1), (b2) The spatial distribution of grid points with different defect concentration at $\bar{c} = 0.1$ and $\bar{c} = 0.3$ in the phase field simulations. (c1)–(c4) The domain structure for $\bar{c} = 0.1$ and $\bar{c} = 0.3$, respectively. (d1)–(d4) The local distribution of ferroelectric phase (T phase and R phase) for $\bar{c} = 0.1$ and $\bar{c} = 0.3$. (e1)–(e12) The Landau free energy for different local compositions for $\bar{c} = 0.1$ and $\bar{c} = 0.3$, respectively.

IV. CONCLUSIONS

In conclusion, we have revealed the necessary conditions for the formation of reentrant relaxors; i.e., phase transition sequence difference (i.e., C to T and C to T to R) at different local compositions (produced by point defect doping) around the interferroelectric T/R phase boundary is essential to the formation of reentrant relaxors. Systematic phase field simulations of a binary ferroelectric system containing a tetragonal (T)/rhombohedral (R) phase boundary, in which local compositional heterogeneity exists, have allowed us to construct a phase diagram that describes normal ferroelectric transition, relaxor transition, and reentrant relaxor transition, which agrees qualitatively with the experimental phase dia-

gram of reentrant relaxor systems and reentrant spin glass systems. Thus, in addition to the local transition temperature effect and local field effect associated with random distributed point defects, which play essential roles in the formation of conventional relaxors, the local transition sequence effect associated with local composition variation around an interferroelectric phase boundary is a necessary condition for the formation of reentrant relaxors. We also find that the unique feature of reentrant relaxors such as the dielectric dispersion below the Curie temperature is correlated with the appearance of R nanodomains in T microdomains upon cooling. This work may also shed light on the formation of other reentrant ferroic glasses and guide the designing of high-performance reentrant relaxors.

[1] V. V. Shvartsman and D. C. Lupascu, Lead-free relaxor ferroelectrics, J. Am. Ceram. Soc. **95**, 1 (2012).

[2] L. E. Cross, Relaxor ferroelectrics, Ferroelectrics **76**, 241 (1987).

[3] D. Sherrington, A spin glass perspective on ferroic glasses, Phys. Status Solidi B **251**, 1967 (2014).

[4] X. R. Ren, Strain glass and ferroic glass-unusual properties from glassy nano-domains, Phys. Status Solidi B **251**, 1982 (2014).

[5] F. Li, M. J. Cabral, B. Xu, Z. Cheng, E. C. Dickey, J. M. LeBeau, J. Wang, J. Luo, S. Taylor, W. Hackenberger, L. Bellaiche, Z. Xu, L. Q. Chen, T. R. Shrout, and S. Zhang, Giant piezoelectricity of Sm-doped $Pb(Mg_{1/3}Nb_{2/3})O_3 - PbTiO_3$ single crystals, Science **364**, 264 (2019).

[6] D. Wang, S. Hou, Y. Wang, X. D. Ding, S. Ren, X. B. Ren, and Y. Wang, Superelasticity of slim hysteresis over a wide temperature range by nanodomains of martensite, Acta Mater. **66**, 349 (2014).

[7] S. S. N. Bharadwaja, J. R. Kim, H. Ogihara, L. E. Cross, S. Trolier-McKinstry, and C. A. Randall, Critical slowing down mechanism and reentrant dipole glass phenomena in $(1-x)BaTiO_3 - xBiScO_3$ ($0.1 \leqslant x \leqslant 0.4$): The high energy density dielectrics, Phys. Rev. B **83**, 024106 (2011).

[8] B. M. Wang, Y. Liu, P. Ren, B. Xia, K. B. Ruan, J. B. Yi, J. Ding, X. G. Li, and L. Wang, Large Exchange Bias after Zero-Field Cooling from an Unmagnetized State, Phys. Rev. Lett. **106**, 077203 (2011).

[9] D. Sherrington, BZT: A Soft Pseudospin Glass, Phys. Rev. Lett. **111**, 227601 (2013).

[10] D. Wang, Y. Z. Wang, Z. Zhang, and X. B. Ren, Modeling Abnormal Strain States in Ferroelastic Systems: The Role of Point Defects, Phys. Rev. Lett. **105**, 205702 (2010).

[11] D. Sherrington, $Pb(Mg_{1/3}Nb_{2/3})$: A minimal induced-moment soft pseudospin glass perspective, Phys. Rev. B **89**, 064105 (2014).

[12] D. Phelan, C. Stock, J. A. Rodriguez-Rivera, S. X. Chi, J. Leao, X. F. Long, Y. J. Xie, A. A. Bokov, Z. G. Ye, P. Ganesh, and P. M. Gehting, Role of random electric fields in relaxors, Proc. Natl. Acad. Sci. USA **111**, 1754 (2014).

[13] Z. K. Hong, X. Q. Ke, D. Wang, S. Yang, X. B. Ren, and Y. Z. Wang, Role of point defects in the formation of relaxor ferroelectrics, Acta Mater. **225**, 117558 (2022).

[14] J. Shen, H. P. Zhang, Z. Q. Chen, L. F. Ouyang, F. R. Wang, Z. Lu, M. Z. Li, Y. H. Sun, H. Y. Bai, and W. H. Wang, The kinetics of reentrant glass transition in metallic liquids, Acta Mater. **244**, 118554 (2023).

[15] S. Ghara, B. G. Jeon, K. Yoo, K. H. Kim, and A. Sundaresan, Reentrant spin-glass state and magnetodielectric effect in the spiral magnet $BiMnFe_2O_6$, Phys. Rev. B **90**, 024413 (2014).

[16] A. H. Pandey, V. R. Reddy, A. K. Nigam, and S. M. Gupta, Investigation of re-entrant relaxor behaviour in lead cobalt niobate ceramic, Acta Mater. **177**, 160 (2019).

[17] A. Surampalli, R. Egli, D. Prajapat, C. Meneghini, and V. R. Reddy, Reentrant phenomenon in the diffuse ferroelectric $BaSn_{0.15}Ti_{0.85}O_3$: Local structure insights and first-order reversal curves study, Phys. Rev. B **104**, 184114 (2021).

[18] M. Viswanathan and P. S. A. Kumar, Observation of reentrant spin glass behavior in $LaCo_{0.5}Ni_{0.5}O_3$, Phys. Rev. B **80**, 012410 (2009).

[19] W. J. Wang, Y. C. Ji, M. X. Fang. D. Wang, S. Ren, K. Otsuka, Y. Z. Wang, and X. B. Ren, Reentrant strain glass transition in Ti-Ni-Cu shape memory alloy, Acta Mater. **226**, 117618 (2022).

[20] S. S. N. Bharadwaja, S. Trolier-McKinstry, L. E. Cross, and C. A. Randall, Reentrant dipole glass properties in $(1-x)BaTiO_3 - xBiScO_3$, $0.1 \leqslant x \leqslant 0.4$, Appl. Phys. Lett. **100**, 022906 (2012).

[21] See Supplemental Material at http://link.aps.org/supplemental/10.1103/PhysRevB.107.224105 for the spatial distribution of defect concentration and the volume fraction of grid points with different c for samples with different parameters used in our simulations; a detailed description on calculating the electric energy density and elastic energy density; the supporting data for the doped ferroelectric phase diagram. Also see Refs. [22,23].

[22] Y. L. Li, L. E. Cross, and L. Q. Chen, A phenomenological thermodynamic potential for $BaTiO_3$ single crystals, J. Appl. Phys. **98**, 064101 (2005).

[23] J. Hlinka and P. Marton, Phenomenological model of a 90° domain wall in $BaTiO_3$ - type ferroelectrics, Phys. Rev. B **74**, 104104 (2006).

[24] S. Wang, M. Yi, and B. X. Xu, A phase-field model of relaxor ferroelectric based on random field theory, Int. J. Solid. Struct. **83**, 142 (2016).

[25] M. D. Glinchuk and R. Farhi, A random field theory model for ferroelectric relaxors, J. Phys.: Condens. Matter **8**, 6985 (1996).

[26] Y. J. Gu, F. Xue, S. M. Lei, T. T. A. Lummen, J. J. Wang, V. Gopalan, and L. Q. Chen, Monoclinic phases arising across thermal inter-ferroelectric phase transitions, Phys. Rev. B **90**, 024104 (2014).

[27] H. B. Huang, G. Z. Zhang, X. Q. Ma, D. S. Liang, J. J. Wang, Y. Liu, Q. Wang, and L. Q. Chen, Size effect of electrocaloric cooling in ferroelectric nanowires, J. Am. Ceram. Soc. **101**, 1566 (2018).

[28] A. Kholkin, A. Morozovska, D. Kiselev, I. Bdikin, B. Rodriguez, P. Wu, A. Bokov, Z. G. Ye, B. Dkhil, L. Q. Chen, M. Kosec, and S. V. Kalinin, Surface domain structures and mesoscopic phase transition in relaxor ferroelectrics, Adv. Funct. Mater. **21**, 1977 (2011).

[29] S. V. Kalinin, B. J. Rodriguez, J. D. Budai, S. Jesse, A. N. Morozovska, A. A. Bokov, and Z. G. Ye, Direct evidence of mesoscopic dynamic heterogeneities at the surfaces of ergodic ferroelectric relaxor, Phys. Rev. B **81**, 064107 (2010).

[30] A. N. Morozovska, E. A. Eliseev, J. J. Wang, G. S. Svechnikov, Y. M. Vysochanskii, V. Gopalan, and L. Q. Chen, Phase diagram and domain splitting in thin ferroelectric films with incommensurate phase, Phys. Rev. B **81**, 195437 (2010).

[31] A. N. Morozovska, E. A. Eliseev, S. V. Svechnikov, A. D. Krutov, V. Y. Shur, A. Y. Borisevich, P. Maksymovych, and S. V. Kalinin, Finite size and intrinsic field effect on the polar-active properties of ferroelectric-semiconductor heterostructures, Phys. Rev. B **81**, 205308 (2010).

[32] S. Choudhury, Y. L. Li, C. E. Krill, III, and L. Q. Chen, Phase-field simulation of polarization switching and domain evolution in ferroelectric polycrystals, Acta. Mater. **53**, 5313 (2005).

[33] Y. L. Li, S. Y. Hu, Z. K. Liu, and L. Q. Chen, Effect of electrical boundary conditions on ferroelectric domain structures in thin films, Appl. Phys. Lett. **81**. 427 (2022).

[34] J. Hlinka, Mobility of ferroelastic domain walls in barium titanate, Ferroelectrics **349**, 49 (2007).

[35] N. Sahu, M. Kar, and S. Panigrahi, Rietveld refinement, microstructure and electrical properties of $PbTiO_3$ ceramic materials, Arch. Phys. Res. **1**, 75 (2010).

[36] X. Dai, A. Digiovanni, and D. Viehland, Dielectric properties of tetragonal lanthanum modified lead zirconate titanate ceramics, J. Appl. Phys. **74**, 3399 (1993).

[37] T. Maiti, R. Guo, and A. S. Bhalla, Evaluation of experimental resume of $BaZr_xTi_{1-x}O_3$ with perspective to ferroelectric relaxor family: An overview, Ferroelectrics **425**, 4 (2011).

[38] M. X. Fang, Y. C. Ji, Z. Zhang, Y. D. Yang, C. Liu, D. Wang, L. X. Zhang, J. H. Gao, and X. B. Ren, Reentrant relaxor–ferroelectric composite showing exceptional electromechanical properties, NPG Asia Mater. **10**, 1029 (2018).

[39] J. H. Gao, Y. Wang, Y. B. Liu, X. H. Hu, X. Q. Ke, L. S. Zhong, Y. T. He, and X. B. Ren, Enhancing dielectric permittivity for energy-storage devices through tricritical phenomenon, Sci. Rep. **7**, 40916 (2017).

[40] A. A. Bokov and Z. G. Ye, Recent progress in relaxor ferroelectrics with perovskite structure, J. Mater. Sci. **41**, 31 (2006).

[41] A. I. Spitsin, A. A. Bush, V. I. Kozlov, A. V. Stepanov, K. E. Kamentsev, and E. A. Tishchenko, Effect of composition on the dielectric properties of $1-x$Ba$(Ti_{0.75}Sn_{0.25})O_3 \cdot x$PbTiO$_3$ solid solutions, Inorg. Mater. **56**, 297 (2020).

[42] J. R. Childress and C. L. Chien, Reentrant magnetic behavior in fcc Co-Cu alloys, Phys. Rev. B **43**, 8089 (1991).

[43] Y. Yang, Y. Ji, M. Fang, Z. Zhou, L. Zhang, and X. Ren, Morphotropic Relaxor Boundary in a Relaxor System Showing Enhancement of Electrostrain and Dielectric Permittivity, Phys. Rev. Lett. **123**, 137601 (2019).

[44] T. Y. Li, C. Liu, X. Q. Ke, X. Liu, L. He, P. Shi, X. Ren, Y. Wang, and X. Lou, High electrostrictive strain in lead-free relaxors near the morphotropic phase boundary, Acta Mater. **182**, 39 (2020).

[45] R. Guo, A. S. Bhalla, C. A. Randall, Z. P. Chang, and L. E. Cross, Polarization mechanisms of morphotropic phase boundary lead barium niobate (PBN) compositions, J. Appl. Phys. **67**, 1453 (1990).